University of Central Florida
STARS

Honors in the Major Theses

Campus Access

Climate Modeling, Outgoing Longwave Radiation, and Tropical Cyclone Forecasting

2018

Thomas Rechtman

Find similar works at: http://stars.library.ucf.edu/honorstheses

University of Central Florida Libraries http://library.ucf.edu

University of Central Florida STARS Showcase of Text, Archives, Research & Scholarship

CLIMATE MODELING, OUTGOING LONGWAVE RADIATION, AND TROPICAL CYCLONE FORECASTING

by

THOMAS RECHTMAN

A thesis submitted in partial fulfillment of the requirements
for the Honors in the Major Program in Mathematics
in the College of Sciences
and the Burnett Honors College
at the University of Central Florida
Orlando, Florida

Spring Term, 2018

Thesis Chair: Ram Mohapatra, Ph.D.

Abstract

Climate modeling and tropical cyclone forecasting are two significant issues that are continuously being improved upon for more accurate weather forecasting and preparedness. In this thesis, we have studied three climate models and formulated a new model with a view to determine the outgoing longwave radiation (OLR) budget at the top of the atmosphere (TOA) as observed by the National Oceanic and Atmospheric Administration's (NOAA) satellite based Advanced Very High Resolution Radiometer (AVHRR). In 2006, *Karnauskas* proposed the African meridional OLR as an Atlantic hurricane predictor, the relation was further proven in 2016 by *Karnauskas and Li*. Here we have considered a similar study for all other tropical cyclone basins.

Dedication

To Mima and Aba. Thank you for getting me here.

Acknowledgements

I would like to thank my mentor and advisor Dr. Ram Mohapatra for guiding me through this journey as well as the McNair Scholar Program for all the support and encouragement.

Contents

List of Figures

List of Tables

Chapter 1: Introduction

Climate modeling using a variety of statistical methods have been used to predict hurricanes and the effects of global warming. The Paris accord set expectations to most countries as to how each will contribute in mitigating the rate of climate change, by limiting their greenhouse gas emissions. However, some people in a position of authority have questioned the ability of science to correctly predict climate change [31].

A famously referenced saying: "all models are wrong, but some are useful", misleads the wider public to distrust mathematical models all together. Yet, the center of the discussion is entirely dependent on the causes and effects of physical, chemical and biological processes, all of which are well understood. These are used as building blocks for models, beginning with the dynamics and physics of the climate system and continuously improving the accuracy of the model by including the more complex processes into our numerical solutions.

In order to fully understand the system and be sure of the accuracy of such models, it is necessary to gather data from terrestrial observations. The recent geologic past is known from the Antarctic ice sheet ice core data, this data indicates that the earth's climate has large variations in geologic time scales. The records we have extend 800,000 years into the past, revealing eight ice ages and interglacials. The variations, we have temperature ranges from $-10°$C to $+4°$C from the modern baseline; we are currently at $+1°$C. The atmospheric concentration of CO_2 varies from 180 parts per million (ppm) to 300 ppm, currently the CO_2 atmospheric concentration is at 408 ppm. Compiling a record of direct observations of weather and climate began in the 1850's.

After World War II, weather balloons measuring temperature, pressure, humidity, and wind velocity were launched at major airports. Shortly after the inception of the United Nations (UN), the World Meteorological Organization (WMO) was formed in 1950 as a specialized agency within the UN. Since then, many measurement campaigns have been put

together to advance the understanding of climate and weather phenomena. Satellite data since 1979 has included measurements on radiation budget, sea surface temperatures, ice extent and has developed further since then. Although, the first weather satellite, Vanguard 2, was launched 1959. With its subsequent missions improving in instrumentation, it was only in 1979 that the data sets brought a full picture of earth's climate system. Ground based data on the other hand, is largely restricted to continental land masses with fewer measurements for the oceans. Ships do record meteorological observations, such as pressure, air temperature, sea surface temperature, and wind velocity. However, ocean vessel routes do not form a uniform coverage, nor they continuously observe a single point in the ocean. Buoys may aid with some the short comings however, there are not enough of them deployed to obtain a sensible data set.

In the first part of this thesis we will be looking into three models related to the atmosphere's thermal structure, in order to formulate a model of outgoing longwave radiation. This is achieved through understanding the radiation balance between the absorption, reflection, and scattering of incoming solar radiation. Generally, we can divide radiation in the atmosphere into two forms: shortwave and longwave. Shortwave radiation in the range between 0.2 and $4\mu m$, is the sunshine that heats the earth. Whereas the cooling effect of the planet is due to the "release" of longwave radiation, which is mostly infrared ranging from 4 to $100\mu m$. Hence we have that the flux at the top of the atmosphere is exclusively shortwave, because other types of radiation do not enter the atmosphere. Some wavelengths can be absorbed or reflected by clouds, gases, and the earth's surface.

Nevertheless, the energy balance over a year is not zero. For instance, the difference between absorbed solar radiation and outgoing longwave radiation varies by approximately $20W/m^2$ a year[18]. This imbalance is due to the fact that the earth stores a certain amount of energy. The heat capacity of the oceans play a significant role in the absorption of radiation, as well as the atmospheric composition. In figure 1.1 we see an illustration of how

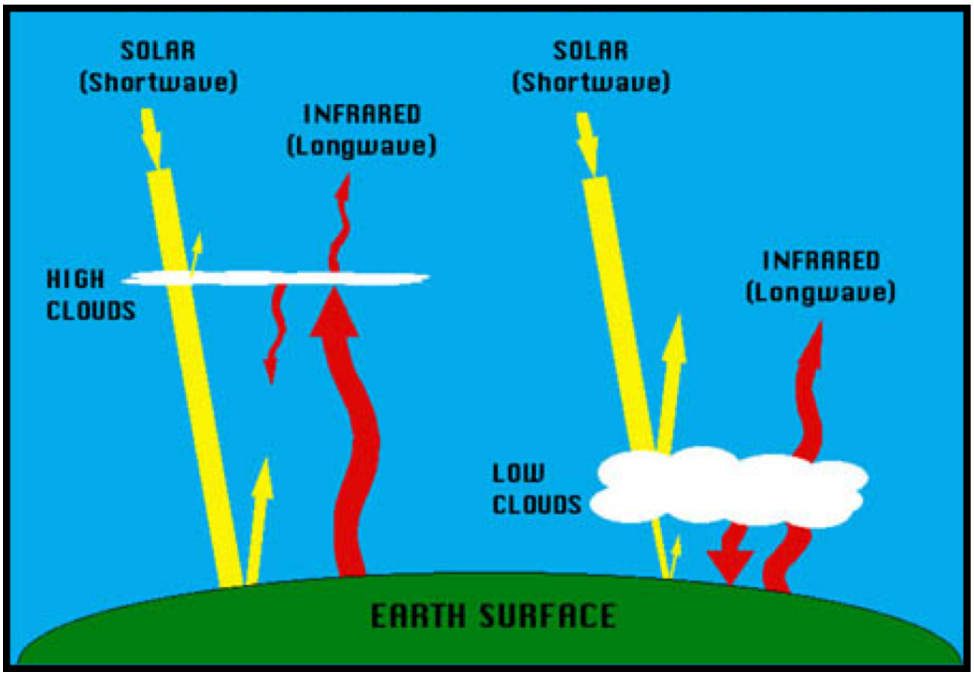

Figure 1.1: Illustration of incoming and outgoing radiation

clouds are able to reflect some of the thermal energy back towards earth; moreover, some atmospheric gases namely greenhouse gases perform the same task which leads to global warming. It has been conjectured that the earth is not currently in radiation balance but going through a trasient phase [31]. How much out of balance? Is a fundamental question in order to determine the timing and extent of human induced climate change.

Our interests in OLR go further then simply modeling earth's radiation budget. It has been shown that longwave radiation over the African continent is capable of predicting season Atlantic hurricane activity (i.e. number of hurricanes per year) [34]. It has also been shown that the observed longwave trends over Africa are been influenced by greenhouse gas emissions [36]. Thus, in this thesis we propose that similar correlations can be found between longwave radiation and tropical cyclone (i.e hurricane, typhoon) activity in the other basins around the world.

Chapter 2: Models

In this chapter will present three different models that represent how our climate behaves in terms of longwave radiation. First, we see a simple model of outgoing radiation as a part of the net radiation budget in the Earth's climate system. Second, we explore part of the Intergovernmental Panel for Climate Change (IPCC) Assessment Report 5 (AR5) ordered models. Finally, in section 2.2 we explore the radiation forcing caused by greenhouse gases, mainly CO_2.

2.1: Simple Outgoing Longwave Radiation (OLR) Model

In 1993 Lagouarde and Brunet proposed a simple model to be evaluated by the NOAA satellite based Advanced Very High Resolution Radiometer (AVHRR)[7], the model examined the surface OLR flux through the following equations.

$$R_n = (1-a)R_g + \varepsilon R_a - L\uparrow \tag{2.1}$$

$$L\uparrow = \varepsilon\sigma T_s^4 \tag{2.2}$$

(2.1) is valid for any time frame, for the purposes of this study we will use daily scales. Thus for this time scale will consider R_s to be

$$R_s = \int_0^\tau \sigma T_s^4 dt \tag{2.3}$$

where $\tau = 24$ hours in a day, and is related to $L\uparrow$ by a version of (2.2)

$$L\uparrow = \varepsilon R_s \tag{2.4}$$

The surface temperature T_s at time t can be described as

$$T_s = T_{am} + \alpha \Delta T \sin\left(\pi \frac{t - t_{SR}}{t_{SS} - t_{SR}}\right) \tag{2.5}$$

with

$$\alpha = \begin{cases} \text{constant} & t_{SR} \leq t \leq t_{SS} \\ 0 & \text{otherwise} \end{cases}$$

Combining (2.3) and (2.5) and integrating the latter we obtain

$$R_s = \sigma T_{am}^4 (\gamma(t_{SR} - t_{SS}) + \tau) \tag{2.6}$$

with

$$\gamma = \frac{3}{8}c^4 + \frac{16}{3\pi}c^3 + 3c^2 + \frac{8}{\pi}c \tag{2.7}$$

and

$$c = \alpha \frac{\Delta T}{T_{am}} \tag{2.8}$$

R_n	Net Radiation Flux
R_g	Incident Solar Radiation
R_a	Incoming Atmospheric Longwave Radiation at Surface
R_s	Surface Black-Body Emission
$L\uparrow$	Surface Upward Longwave Radiation
a	Albedo
σ	Stephen-Boltzmann constant
ε	Emissivity
T_s	Surface Temperature

Table 2.1: Net radiation model variables and coefficients

2.2: Coupled Model Intercomparison Project's CO_2 Forcing

The phase 5 of the Coupled Model Intercomparison Project (CMIP5) had as one of its goals to better understand processes related to the carbon cycle and clouds. In 2013 *Geoffroy*

et al. proposed an analytical solution to 16 of the atmosphere-ocean global climate models (AOGCMs).

2.2.1 Atmosphere, Land Surface, and Upper-Ocean

The annual mean surface temperature is extremely useful when determining effects of climate change induced by an external perturbation.

Energy-balance models (EBMs) are simple climate models (SCMs) that can be helpful when summarizing particular properties of the more complicated AOGCMs. In [29] a two-layer EBM is proposed to analyze thermal proprieties in CMIP5 models.

The net radiative imbalance N can be expressed as $N = \mathcal{F} - \lambda T$. Furthermore in equilibrium, when $N = 0$ we obtain the equilibrium temperature $T_{eq} = \mathcal{F}/\lambda$.

The two predictive variables T and T_0, the forcing parameter $\mathcal{F}$ and four free parameters γ, λ, C, and C_0; satisfy the system:

$$C\frac{dT}{dt} = \mathcal{F} - \lambda T - \gamma(T - T_0) \tag{2.9}$$

$$C_0\frac{dT_0}{dt} = \gamma(T - T_0) \tag{2.10}$$

In the case for this particular model, the outside perturbations are forced from CO_2 concentrations. Thus, the radiative forcing becomes as follows:

$$\mathcal{F}(t) = \frac{\mathcal{F}_{2\times CO_2}}{\log(2)} \log\left(\frac{[CO_2]_t}{[CO_2]_0}\right) \tag{2.11}$$

where $[CO_2]_t$ and $[CO_2]_0$ are the time dependent and preindustrial CO_2 concentrations respectively and $\mathcal{F}_{2\times CO_2}$ is the radiative forcing with doubling the concentration of carbon dioxide in the atmosphere. The right hand side of (2.9), (2.10) are the tendencies of heat contents in each layer.

The temperature T_H is defined as the climate systems heat uptake, in other words, it is

the difference between T and T_{eq}. Therefore, T_H is the storage of heat in the climate system at any time, following the equation.

$$T_H(t) = T(t) - T_{eq}(t) = -\frac{1}{\lambda}\left(C\frac{dT}{dt} + C_0\frac{dT_0}{dt}\right) \tag{2.12}$$

Notice that here when $T_H < 0$, it represents positive heat storage in the climate system.

T	Global mean surface air temperature perturbation
T_0	Characteristic temperature perturbation of the deep-ocean
$\mathcal{F}$	Radiative forcing
N	Net radiative imbalance
λ	Radiative feedback parameter
γ	Heat exchange coefficient
C	Upper-ocean heat capacity
C_0	Deep-ocean heat capacity

Table 2.2: EBM variables and parameters

2.2.2 Deep Ocean

Following the set up of the upper-ocean model above, the framework is taken and improved upon to generalize for the heat uptake of the deep ocean, both in general and for localized regions. (2.9) is slightly modified by the addition of the deep-ocean heat uptake efficacy factor ε making it

$$C\frac{dT}{dt} = \mathcal{F} - \lambda T - \varepsilon\gamma(T - T_0) \tag{2.13}$$

while (2.10) remains unchanged. Furthermore we define $H = \gamma(T - T_0)$ as the heat flux exchange between the upper and deep ocean layers, which then further changes the net radiative imbalance at the top of the atmosphere (TOA).

$$N = \mathcal{F} - \lambda T - (\varepsilon - 1)H \tag{2.14}$$

Geoffroy et al. in [28] goes further to hypothesize that the net radiative imbalance is the

sum of the instantaneous heat uptakes.

$$N = C\frac{dT}{dt} + C_0\frac{dT_0}{dt} \tag{2.15}$$

On the other hand, we are also able to describe the net radiative imbalance as the sum of the radiative forcing and radiative response (R_T).

$$N = \mathcal{F} + R_T \tag{2.16}$$

The radiative response R_T, in turn, can be described as the sum of three radiative responses $R_{eq} = -\mathcal{F}$ and the responses R_U and R_D equal to the instantaneous rate of heat storage in the two layers of the system. The temperature changes in the upper ocean T_U and deep ocean T_D are then introduced accordingly, such that R_U and R_D are linear functions of each with feedback parameters λ and λ_D, respectively. Leading to the system of equations:

$$-\mathcal{F} = R_{eq} = -\lambda T_{eq} \tag{2.17}$$

$$C\frac{dT}{dt} = R_U = -\lambda T \tag{2.18}$$

$$C_0\frac{T_0}{dt} = H = R_D = -\lambda_D T_D \tag{2.19}$$

The deep-ocean heat uptake is related to a different feedback parameter due to the patterns in T_D (for more details see [28] section 2b).

Likewise, additivity of surface air temperature response is assumed yielding:

$$T = T_{eq} + T_U + T_D \tag{2.20}$$

We see the assumption to be valid as it yields the total heat uptake of the system $T_H =$

$T - T_{eq} = T_u + T_D$, we also see that the sum of the upper and deep ocean radiative responses form the net radiative imbalance in the system: $R_U + R_D = N$.

Now by combining (2.17), (2.18), (2.19), and (2.20) we obtain

$$C\frac{dT}{dt} + H = \mathcal{F} - \lambda T - (\lambda - \lambda_D)T_D \tag{2.21}$$

the deep-ocean heat uptake efficacy factor is then introduced following [21], [24], [37].

$$\varepsilon = \frac{\lambda}{\lambda_D} \tag{2.22}$$

Take this definition into account and the fact that $T_D = -H/\lambda_D$ we have that (2.13) is equivalent to (2.21).

It is often useful to examine the local energy balance to understand feedback response of the temperature, the change in heat content of a climate system column is equal to the local radiative imbalance and the local convergence of the horizontal energy.

$$\frac{dh^i}{dt} + \frac{dh_0^i}{dt} = \mathcal{F}^i - \lambda^i T^i + A_t^i + A_{0t}^i \tag{2.23}$$

dh^i/dt	Local change in heat of upper-ocean
$dh_0^i dt$	Local change in heat of deep-ocean
A_t^i	Local convergence of horizontal energy flux of upper-ocean
A_{0t}^i	Local convergence of horizontal energy flux of deep-ocean

Table 2.3: local energy balance variables

Other variables still hold the same meaning with the superscript i representing the local value, and the subscripts eq, U, and D still representing equilibrium, upper-ocean and deep-

ocean respectively. We have that the averages of the introduced local variables are

$$\frac{1}{n}\sum_{i=1}^{n}\frac{dh^i}{dt} = C\frac{dT}{dt}$$

$$\frac{1}{n}\sum_{i=1}^{n}\frac{dh_0^i}{dt} = C\frac{dT_0}{dt}$$

and

$$\frac{1}{n}\sum_{i=1}^{n}A_t^i = \frac{1}{n}\sum_{i=1}^{n}A_{0t}^i = 0$$

Furthermore, note that the local heat flux between the two layers satisfies

$$\frac{dh_0^i}{dt} = H^i + A_{0t}^i \tag{2.24}$$

The assumption of additivity for the temperature balance continues and due to this assumption we are able to decompose (2.23) as

$$\mathcal{F}^i - \lambda^i T_{eq}^i + A_{eq}^i + A_{0eq}^i = 0 \tag{2.25}$$

$$-\frac{dh^i}{dt} - \lambda^i T_U^i + A_U^i + A_{0U}^i = 0 \tag{2.26}$$

and

$$-\frac{dh_0^i}{dt} - \lambda^i T_D^i + A_D^i + A_{0D}^i = 0 \tag{2.27}$$

The additivity assumption also follows for the local convergence of horizontal energy flux variables and the equilibrium, upper and deep ocean components of the variables also average to zero. Assuming that $A_{0U}^i = 0$ leads to $A_{0D}^i = A_{0t}^i - A_{0eq}^i$.

The function $r_{eq}^i = T_{eq}^i/T_{eq}$ is introduced as the normalized equilibrium temperature

amplitude function. Allowing us to rewrite the local heat budget at equilibrium as

$$\mathcal{F}^i - \lambda^i r^i_{eq} T_{eq} + A^i_{eq} + A^i_{0eq} = 0 \tag{2.28}$$

Note that the equilibrium temperature depends on local forcing, feedback, and amplitude of local energy convergence. Hence, the total feedback is determined to be

$$\lambda = \frac{1}{S} \int \int r^i_{eq} \lambda^i ds \tag{2.29}$$

where S is the world's surface area and ds is the surface element. Likewise the deep-ocean heat uptake feedback parameter can similarly be described as

$$\lambda_D = \frac{1}{S} \int \int r^i_D \lambda^i ds$$

where $r^i_D \neq r^i_{eq}$, for more information refer to (2.19).

From (2.19) and (2.22) we can express the net radiative imbalance as

$$N = \mathcal{F} - \lambda T - (\lambda - \lambda_D) \frac{\varepsilon}{\lambda} H \tag{2.30}$$

the TOA radiative flux can be described in two separate components shortwave (SW) and longwave (LW). These variables and radiative parameters can be introduced to each component individually yielding the two equations

$$N^{SW} = \mathcal{F}^{SW} - \lambda^{SW} T - (\lambda^{SW} - \lambda^{SW}_D) \frac{\varepsilon}{\lambda} H \tag{2.31}$$

$$N^{LW} = \mathcal{F}^{LW} - \lambda^{LW} T - (\lambda^{LW} - \lambda^{LW}_D) \frac{\varepsilon}{\lambda} H \tag{2.32}$$

Each of these parameters are calculated and described in [28] according to the 16 AOGCMs

from CMIP5

2.3: Cloud Radiation Forcing

2.3.1 Thermodynamics

To understand how clouds work, we must first understand the thermodynamics of water (i.e. moisture) in the atmosphere, how it is quantified and how it moves in the air.

We let ρ_w and ρ_d be the densities of wet (water vapor) and dry air respectively. We say that that $q = \frac{\rho_w}{\rho_d}$ is the mixing ratio of vapor and dry air. Furthermore, the specific humidity of the air is defined as

$$\frac{\rho_w}{\rho_w + \rho_d}$$

Conservation of mass implies that

$$\frac{dq}{dt} = \frac{1}{\rho} M + E$$

where M is a sink, defined as the change through freezing and condensation, and E is a source, as the rate of change through evaporation. The thermodynamic equation is modified due to the release of latent heat as water vapor converts to liquid water

$$C_p dT - \frac{1}{\rho} dp = -L dq_s$$

where T is temperature, p is pressure, and q_s is the saturation mixing ratio. Since we have that $dp = -\rho g dz$, the change in moisture's temperature as we rise in the atmosphere (i.e. lapse rate) becomes

$$\frac{dT}{dz} = -\frac{g}{C_p} - \frac{L}{C_p} \frac{dq_s}{dz} \tag{2.33}$$

We then obtain an approximation by combining the above equation with the Clausius-Claperyon equation [15]

$$\frac{dq_s}{dz} \approx \frac{L q_s}{R_m T^2} \frac{dT}{dz} + \frac{q_s g}{RT} \tag{2.34}$$

thus we get the new moisture lapse rate [31] by using (2.33) and (2.34)

$$\frac{dT}{dz} = -\frac{gR_mT}{R}\left(\frac{RT + Lq_s}{C_pR_mT^2 + L^2q_s}\right) \tag{2.35}$$

More generally the energy budget associated with moisture will enter the system as a source and change of temperature will come from the conversion of vapor to liquid and vice versa over time, thus

$$C_p\frac{dT}{dt} \approx L(q - q_s)$$

C_p	Heat capacity of air	$1.00464 \times 10^3 J(kgK)^{-1}$
L	Latent heat of water vaporization	$2.5104 \times 10^6 J(kg)^{-1}$
g	Earth's gravitational constant	$9.8ms^{-2}$
R	Ideal gas constant	$287.04J(kgK)^{-1}$
R_m	Gas constant of water vapor	$461J(kgK)^{-1}$

Table 2.4: Coefficients and their values

2.3.2 Cloud and Radiation Models

In a 1997 study different cloud radiation schemes were tested in the National Center for Atmospheric Research (NCAR) Community Climate Model Version 2 (CCM2). The scheme we are most interested in is the one of clouds with variable droplet effective radius including the ice phase (CWRI), which is the one built upon all previous schemes as described in [13].

Cloud water content is represented through the simple equation

$$q_w = q + q_c$$

where q_w is the total water content, q is the specific humidity as seen previously, and q_c represents the cloud water content. In the model used these are defined through statistical methods of a simple symmetric triangular distribution function [38].

An assumption made is that a cloud's radiative properties are dependent on their water

content, thus the cloud water path (CWP) is computed in explicit terms based on the above scheme

$$\text{CWP} = \int \rho_w dz = \frac{q_c}{C}\rho_a \Delta z \tag{2.36}$$

here CWP is in kg m^{-2}, ρ_w is the cloud water density in kg m^{-3}, C is the fraction being observed, hence the fraction is the in-cloud water content, ρ_a is the air density and Δz is the atmospheric layer.

In addition to the cloud water path's dependence on the cloud water content, the effective radius for water liquid water droplets is parametrized as

$$r_L = \left(\text{LWC} \times \frac{3}{4\pi N}\right)^{\frac{1}{3}} \tag{2.37}$$

the radius r_L is in μm, LWC represents the **liquid water content** with units gm^{-3} and N is an estimate of the concentration of droplets to be taken as 150cm^{-3} over oceans and 600cm^{-3} over land. On the other hand, the effective droplet radius for an ice cloud can be described in terms of temperature as shown in [3], [10], so we use

$$r_I = 0.71T + 61.29 \tag{2.38}$$

r_I follows the same units as r_L, T is in °C, however, there are boundaries associated with r_I, $4\mu\text{m} \leq r_I \leq 40\mu\text{m}$, for reasons associated with absorption and scattering which were not covered here but are in [13]. In temperatures where we can find both ice and liquid water in a cloud the following function was formulated

$$f = \begin{cases} \frac{1}{6}\left(\frac{T+15}{5}\right)^2 & -15°\text{C} < T < -5°\text{C} \\ 1 - \frac{1}{3}\left(\frac{T}{5}\right)^2 & -5°\text{C} \leq T < 0°\text{C} \end{cases}$$

thus the resulting mixed phased radius r_m can be written as

$$r_m = f r_L + (1 - f) r_I \tag{2.39}$$

For the purposes of this thesis we mostly concentrate on the longwave radiation components of the presented models. So, for longwave radiation we must understand the emissivity of a cloud $\boldsymbol{\epsilon}$, which is defined in each layer k (i.e. each Δz) in terms of CWP [9]

$$\boldsymbol{\epsilon}(k) = 1 - \exp(a\mathrm{CWP}(k)) \tag{2.40}$$

with a being an absorption coefficient which takes the value 0.065 $\mathrm{m^2 g^{-1}}$ for ice clouds and $0.13\mathrm{m^2 g^{-1}}$ for water clouds.

Moreover, understanding the more straightforward link between cloud cover and the radiation budget, we must address cloud radiation forcing (CF) [4], [6]. CF is defined as the impact of clouds with regards to radiation budget at the top of the atmosphere, which can be expressed as

$$\mathrm{CF} = (Q - Q_C) - (F - F_C)$$

where Q is the net incoming solar radiation, F is the outgoing longwave radiation at TOA, and the subscript C denotes the radiation flux during clear skies for both. Similarly to section 2.2.2 we can split CF into longwave (LW) and shortwave (SW).

$$\mathrm{CF}_{LW} = F_C - F$$

Although, here we are not too concerned in isolating the longwave feedback it is worth mentioning that it is possible to decompose the total OLR. The ΔF due to climate change may be decomposed into variations of temperature (T), water vapor (q), clouds (CL), and

more, in other words

$$\Delta F = \Delta F_T + \Delta F_q + \Delta F_{\text{CL}} + \cdots + R_e \tag{2.41}$$

R_e is what we call the residual term, and ΔF_{CL} is the change in quantity arising form the simulation with respect to clouds.

2.4: Proposed Outgoing Longwave Radiation Model

Here, we will propose a model that will strictly compute the outgoing longwave radiation at the top of the atmosphere. We will quite literally combine the three models above to provide a simple, yet complete picture of OLR from Earth's climate system. Furthermore, the model will concentrate on localized areas as the land scape of the earth changes.

We have that the OLR coming from earth follows the Stephen-Boltzmann Law of black-body radiation with regards to emission thus

$$\text{OLR} = \boldsymbol{\epsilon}\sigma \int T_o dt. \tag{2.42}$$

Here T_o represents the temperature at the medium measured. Those could be land (l), upper ocean (u), or cloud (c). The temperature of deep ocean (d) will also be taken into consideration as it influences the temperature of the upper ocean.

Assumption 1: the net radiative imbalance can be expressed as the difference between radiation forcing and the temperatures radiative feed back $N = \mathcal{F} - \lambda T$. Following from *Geoffroy et al.* $\mathcal{F}$ is the CO_2 forcing expressed over time as:

$$\mathcal{F}(t) = \frac{\mathcal{F}_{N\times \text{CO}_2}}{\log(2)} \log\left(\frac{[\text{CO}_2]_t}{[\text{CO}_2]_0}\right). \tag{2.43}$$

Where $\mathcal{F}_{N\times \text{CO}_2}$ is the average radiative forcing of placing N times the preindustrial amount of CO_2 into the atmosphere. $[\text{CO}_2]_t$ is the carbon dioxide concentration in the atmosphere, and $[\text{CO}_2]_0$ is the preindustrial concentration (this holds true for $t \leq 0$).

Assumption 2: the atmosphere does not play a significant role in emitting radiation. Hence we obtain a differential equation for the lands heat.

$$C_l \frac{dT_l}{dt} = \mathcal{F} - \lambda T_l. \tag{2.44}$$

Assumption 3: Sea ice does not have an effect in the in ocean temperatures, with this assumption we are ready to propose the system as found in [28].

$$\begin{cases} C_u \frac{dT_u}{dt} = \mathcal{F} - \lambda T_u - \delta\gamma(T_u - T_d) \\ C_d \frac{dT_d}{dt} = \delta\gamma(T_u - T_d). \end{cases} \tag{2.45}$$

We can express this system in matrix form as

$$\frac{d}{dt}\begin{bmatrix} T_u \\ T_d \end{bmatrix} = \begin{bmatrix} -(\lambda+\delta\gamma)/C_u & \delta\gamma/C_u \\ \delta\gamma/C_u & -\delta\gamma/C_u \end{bmatrix}\begin{bmatrix} T_u \\ T_d \end{bmatrix} + \begin{bmatrix} \mathcal{F}/C_u \\ 0 \end{bmatrix},$$

let us call

$$A = \begin{bmatrix} -(\lambda+\delta\gamma)/C_u & \delta\gamma/C_u \\ \delta\gamma/C_u & -\delta\gamma/C_u \end{bmatrix}.$$

We find that A has eigenvalues of the form $1/e_+$ and $1/e_-$ where

$$e_\pm = \frac{C_u C_d}{2\eta\delta\gamma}\left(\frac{\eta+\delta\gamma}{C_u} + \frac{\delta\gamma}{C_d} \pm \sqrt{\left(\frac{\eta+\delta\gamma}{C_u} + \frac{\delta\gamma}{C_d}\right) - \frac{4\eta\delta\gamma}{C_u C_d}}\right).$$

Furthermore A has eigenvectors of the form $(1, v_+)^T$ and $(1, v_-)^T$ where

$$v_\pm = \frac{C_u}{2\delta\gamma}\left(\frac{\eta+\delta\gamma}{C_u} - \frac{\delta\gamma}{C_d} \pm \sqrt{\left(\frac{\eta+\delta\gamma}{C_u} + \frac{\delta\gamma}{C_d}\right) - \frac{4\eta\delta\gamma}{C_u C_d}}\right).$$

These values will allow us to solve (2.45). The solutions are fairly trivial, in (2.44) we have

a linear differential equation with the following solution

$$T_l(t) = e^{-\lambda t/C_l} T_l(0) + e^{-\lambda t/C_l} \int_0^t e^{\lambda s/C_l} \mathcal{F}(s) ds, \tag{2.46}$$

similarly, we used variation of parameter to solve (2.45)

$$\begin{bmatrix} T_u \\ T_d \end{bmatrix} = e^{tA} \int_0^t (e^{sA})^{-1} \begin{bmatrix} \mathcal{F}(s)/C_u \\ 0 \end{bmatrix} ds. \tag{2.47}$$

We approach cloud radiative emission, proposed by *Lee* as the cloud radiative forcing in [13]. Therefore, we must bring about a new assumption.

Assumption 4: A cloud's radiative properties are dependent on its water content (q_c). We have that a cloud water content is defined as a symmetric triangular distribution function [38]. For more information on the formulation of the model see 2.3.2. Ultimately we use (2.40) to determine the emissivity of a given cloud. Lastly, we use the statistical models as described in [22] and [19] to determine cloud occurrence frequency and temperature respectively.

Therefore, our OLR model will rely on three variables x, the latitudinal coordinate, y, the longitudinal coordinate, and t, the time. The following $\boldsymbol{\epsilon}$ will vary depending on terrain within the coordinates (x, y), or cloud cover.

$$\text{OLR}(x, y, t) = \begin{cases} \boldsymbol{\epsilon}(x, y)\sigma \int_0^t T_l(s) ds & \text{when } x, y \text{ are over land} \\ \boldsymbol{\epsilon}(x, y)\sigma \int_0^t T_u(s) ds & \text{when } x, y \text{ are over ocean} \\ \boldsymbol{\epsilon}\sigma \int_0^t T_u(s) ds & \text{when } x, y \text{ are under cloud cover} \end{cases} \tag{2.48}$$

Chapter 3: Tropical Cyclone Basins

There are seven tropical cyclone basins where large storms occur on a regular basis. According to NOAA's National Hurricane Center, approximately 69% of the tropical cyclones occur in the Northern Hemisphere while only 31% can be found in the Southern Hemisphere. Approximately 12% occur in the Atlantic Ocean, 57% occur in the Pacific and the remaining 31% occur in the Indian Ocean [30].

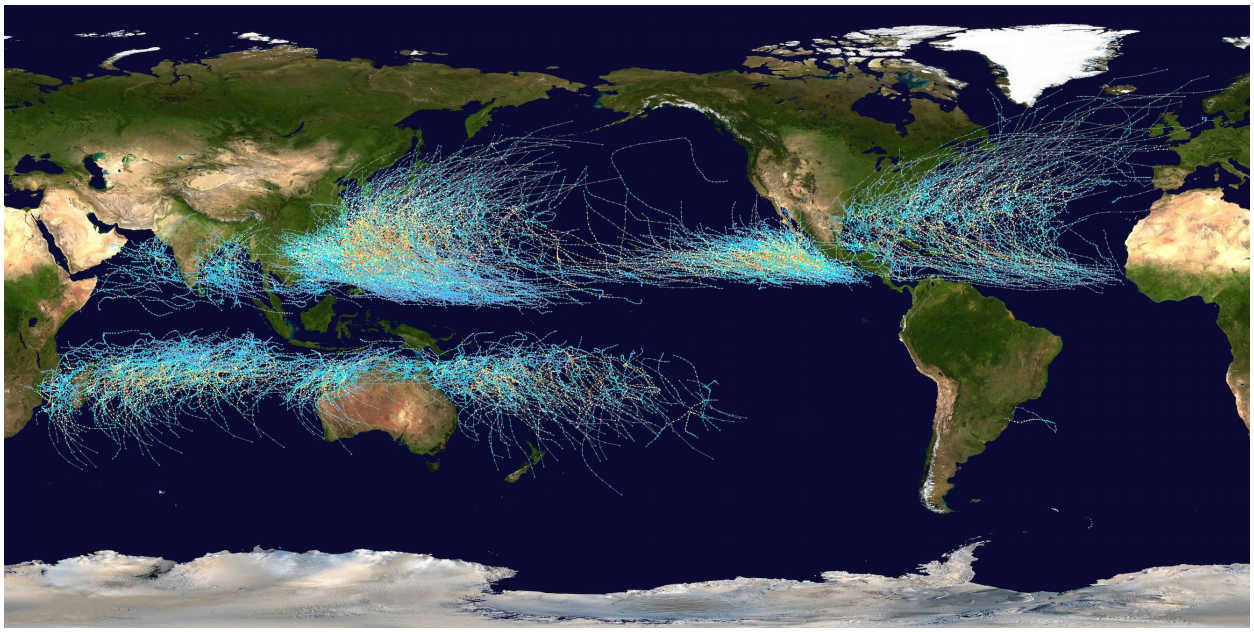

Figure 3.1: Track of all tropical cyclones in the World

3.1: Atlantic

The Atlantic Basin encompasses the Caribbean Sea, Golf of Mexico, and the North Atlantic Ocean. Tropical Cyclones in this region are known as Cape Verde type hurricanes due to their formation off of the coast of North Africa and their ability to affect North America.

Hurricane formation varies greatly within each year. The range of named storms is from 28 to 4 per year [8]. The season in this basin ranges from June 1st to November 30th. The

Atlantic Basin is the third most active region in the world. Due to the unique currents in the Golf of Mexico and the Caribbean Sea, this area experiences some of the largest hurricanes in the world (e.g. *Irma, Katrina*).

3.2: Northeast Pacific

Northeast Pacific Basin which ranges from Mexico and Southern California to the 180° longitude line. Hurricanes in this region originate off the westerly waves by the intertropical convergence zone (ITCZ) from the northern parts of South America.

Most storms in this region are dragged through the ITCZ westward and only a small percentage of the storms reach the coast of Mexico. Throughout history, only one a handful has reached the southwest United States [16]. This basin experiences about as much activity as its Atlantic counterpart, with a similar season from May 15th to November 30th.

3.3: Northwest Pacific

Northwest Pacific (NWP) Basin ranging from the 180° longitude line to East Asia and the South China Sea, is the most active basin. It has an average of 26 tropical storms per year where 16 of of those storms develop in Typhoons/Super Typhoons. They account for one-third of all tropical storm activity on the planet.

Storms here form west of Hawai'i in the Central Pacific and affect virtually every country in East and Southeast Asia. The region experiences tropical activity year round however, it's peak season occurs from May through November.

3.4: North Indian

North Indian Basin includes the Bay of Bengal and the Arabian Sea. This region is extremely inactive with an average of 5.1 storms per year as of 2014 [32]. Typhoons here affect mostly India and Bangladesh however, the storms may reach countries in East Africa and the Arabian Peninsula.

3.5: Southwest Indian

Southwest Indian Basin is the region from Africa to about 100° east. This basin experiences an average of 9 tropical storms per year, most of which affect the island country of Madagascar and other smaller island nations. These storms originate off the western coasts of Australia and Indonesia.

3.6: Southeast Indian

Southeast Indian Basin reaches from 100° east to 142° east. Similarly to the basin mentioned above, storms here form between Australia and Indonesia. The region is slightly less active than its western counterpart.

3.7: Southwest Pacific

Southwest Pacific Basin (142° east to about 120° west). These storms are similar to the Northwest Pacific Basin storms where they develop in the middle of the Pacific Ocean. However, activity is far less in the Southern Hemisphere. All the Southern Basins share the same peak season from November until April.

It is also common to refer to the Southeast/west Indian basins as the Australian basin, as the 142° east longitude line crosses Australia. Cyclones from both basins affect the country.

Chapter 4: Tropical Cyclone Forecasting

The warm oceans in tropical region are the breeding grounds of tropical cyclones. These take different names according to their intensity. A tropical depression has rotary winds under 17ms^{-1}, a tropical storm rotates at speeds under 33ms^{-1} and a fully formed tropical cyclone (i.e. Hurricane, Typhoon) speeds are greater than 33ms^{-1}.

Tropical cyclone (TC) forecasting has been a challenging problem for many decades. This global issue needs to be dealt with in nearly every continent in the planet, as it affects life and property. TC seasonal forecasting is a key element of an early warning system to increase preparedness of coastal communities ahead of the TC season and such a service is provided by several organizations around the world.

4.1: General Forecasting

TC seasonal forecasting, until recently, has concentrated greatly in the connections between sea surface temperature (SST) and TC activity. Granted, it has been well documented that it requires sea surface temperature above 26°C for tropical cyclones to form [1]. The focus in SST pushed for increased knowledge in phenomena such as El Niño Southern Oscillation (ENSO).

ENSO is highly linked to precipitation in certain coastal areas around the globe [5]. Furthermore, ENSO-related covariates for TC seasonal forecasting for a specific region depends on the impact of ENSO on the spatial distribution of TCs. Linear discrimination analysis and support vector regression (SVR) models (or support vector regression machines) are used as forecasting tools, in particular when working with ENSO Index [33].On the other hand, El Niño is highly unpredictable and we do not fully understand why the variability is so much higher in the past century [27].

Furthermore, TC tracking forecast has been prioritized over seasonal and precipitation forecasts; some dynamical models attempt to predict the amount of precipitation of a TC

as it is being tracked [35]. However, with advancements in remote sensing, there is more to anticipate with the amount of precipitation a region may receive[23].

Other parameters explored in tropical cyclone activity forecast are those inter-annual variations of TCs in the Australian Region are linked with pressure anomalies in northern Australia [2]. Furthermore, large scale circulations, including wind shear have been proven to aid in the forecast of tropical cyclones due to the are crucial for cyclogenesis [14], [20].

4.2: Outgoing Longwave Radiation

The latest decades advancements in satellite imagery and remote sensing have allowed us to explore new sets of data and possibilities. One of which shows potential as a predictor of rainfall and tropical cyclones: outgoing longwave radiation (OLR).

OLR has been shown to have a high negative correlation in equatorial and low latitude area in South East Asia; namely Indonesia [25]. This region is the source of tropical activity leading towards the genesis of cyclones in the Southeast and west Indian sea.

Furthermore, OLR has also been shown to be highly linked to Atlantic tropical cyclone activity when in the context of the African meridional OLR [17], [34]. The OLR Index yield a success rate of 87%, compared to NOAA's outlooks of 53%. The indices are statistically robust, highly predictable, and physically linked to TC activity.

4.3: Future of Tropical Activity

The emission of greenhouse gases has put a strain into the environment. As the earth's climate system heats up, the oceans will be warmer and potentially produce more powerful tropical cyclones.

In particular, it has been shown that since 1984, typhoons in East Asia have been gaining in size and speed as well as possibly changing paths [39]. Moreover, [26] shows that at the Western North Pacific Basin, tropical cyclones are decreasing in activity and frequency but, increasing in intensity and efficiency of intensity.

On the other hand, the OLR trend pattern from CMIP5 future projections shows an

increasing OLR gradient in response to the greenhouse gases; suggesting a potential 10%-20% increase in tropical cyclone activity by the end of the twenty first century [36].

Chapter 5: Experiment

5.1: Methods

Measurements of OLR were made by the satellite based Advanced Very High Resolution Radiometer (AVHRR). The AVHRR has flown aboard the National Oceanic and Atmospheric Administration (NOAA) Polar Orbiting Environmental Satellites (POES). Data collected by the NOAA- 7, 9, 11, 12, 14 and 16 satellites are used in the AVHRR OLR data set. Measuring electromagnetic radiation with wavelengths between 10.3 and 12.5 micrometers at a spacial resolution of 4 km, which is used to estimate longwave emissions.

The data have been interpolated in space and time to fill missing values [12]. Moreover, the OLR Index is constructed by the algebraic difference between the maximum and minimum of areas east of the basin being analyzed. In particular, this action is done to avoid a drift signal in satellite OLR measurements[11].

5.2: Results

Using the two-tailed T test for 99% significance we find the following basins to have a correlation coefficient with their respective OLR indexes.

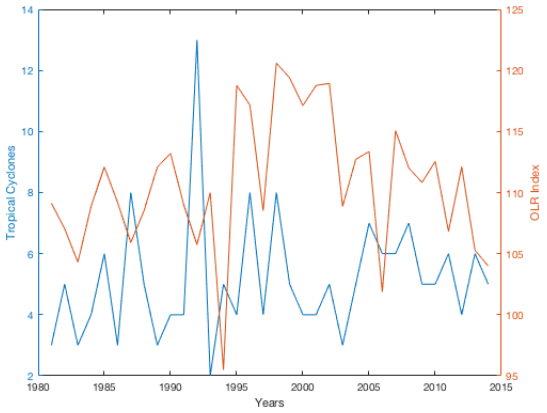

Figure 5.1: North Indian

Within the northern oceans the correlation coefficients are low, with North Indian ocean (Fig.5.1) obtain $r = -0.0221$, Northwest Pacific Ocean (Fig.5.3) has the coefficient $r =$

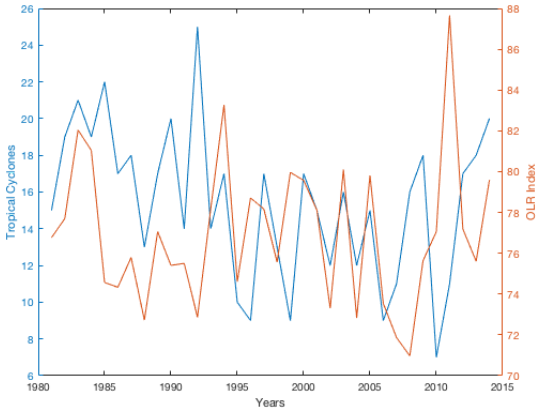

Figure 5.2: Northeast Pacific

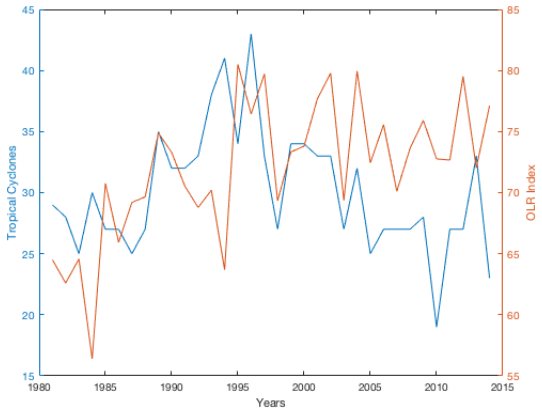

Figure 5.3: Northwest Pacific

0.1255, and the Northeast Pacific Ocean (Fig.5.2) with $r = 0.0287$. However, we observe sections in the East Pacific basin that do align with the OLR index which yields a correlation coefficient $r = 0.5351$ between the years of 1993 and 2006, and if reduced more to the section between 2000 and 2006 the coefficient increases again to $r = 0.8871$. This will be further commented on in the conclusion section.

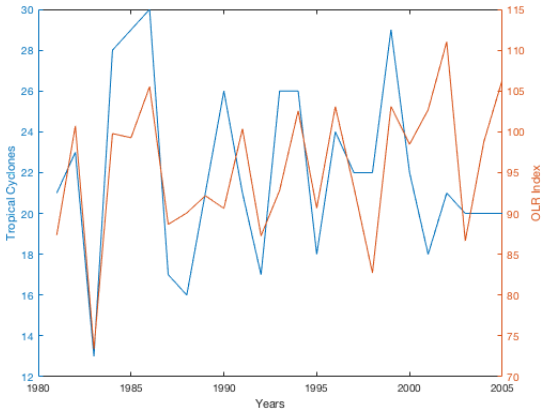

Figure 5.4: South Indian

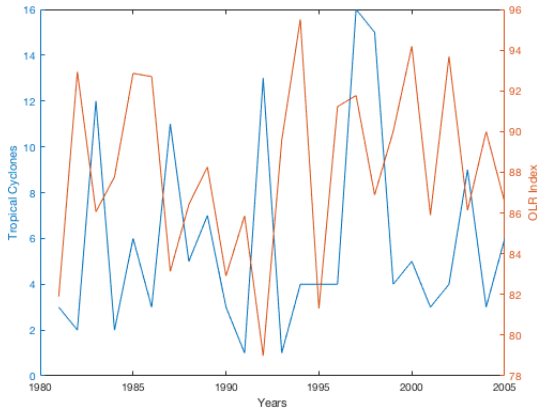

Figure 5.5: South Pacific

The Southern Hemispheric oceans in turn had drastically different results with the South Pacific basin yielding $r = -0.2196$ (Fig.5.5), meanwhile the highest correlation belongs to the South Indian basin with $r = 0.5274$ (Fig.5.4).

Chapter 6: Conclusion

The relatively high correlation found between the OLR index and the South Indian basin suggests that longwave radiation merits further study as a potential predictor for tropical cyclones in that region. Likewise, for the East Pacific basin the patterns between the years 1993/2000 and 2006 are unique to the basin in the sense that no other basin had high correlations in a span longer then four years (except the South Indian). The time frames of these patterns seem to coincide with strong El Niño events, thus further study in the connections between ENSO events and outgoing longwave radiation are of interest as well.

Due to the nature and time constraints in this study the model was only formulated. Thus, it remains for future research to calibrate the model and compare the results with the AVHRR based satellite data. Furthermore, it would be ideal to create analytical functions to model cloud temperature. The use of further satellite data to calibrate cloud top temperature, water path, and occurence frequency as in the International Satellite Cloud Climatology Project (ISCCP) would be necessary for accurate results. Lastly, to make the model comprehensive it is imperative that the interaction between the ocean and sea ice be added to the equations in order to portray all the regions in the world to its full extent.

Bibliography

[1] E. Palmén, "On the Formation and Structure of Tropical Hurricanes," *Geophysica*, vol. 3, pp. 26–38, 1948.

[2] N. Nicholls, "A Possible Method for Predicting Seasonal Tropical Cyclone Activity in the Australian Region," *Monthly Weather Review*, vol. 107, no. 9, pp. 1221–1224, Jul. 1979.

[3] A. J. Heymsfield and C. M. R. Platt, "A parameterization of the particle size spectrum of ice clouds in terms of the ambient temperature and the ice water content," *Journal of the Atmospheric Sciences*, vol. 41, no. 5, pp. 846–855, 1984.

[4] V. Ramanathan, "Role of earth radiation budget studies in climate and general circulation research," *J. Geophys. Res.; (United States)*, Apr. 1987.

[5] C. Ropelewski and M. Halpert, "Global and Regional Scale Precipitation Patterns Associated with the El Niño Souther Oscillation," *Monthly Weather Review*, 1987.

[6] V. Ramanathan, B. R. Barkstrom, and E. F. Harrison, "Climate and the earth's radiation budget.," *Physics Today*, no. 5, p. 22, 1989.

[7] J. P. LAGOUARDE and Y. BRUNET, "A simple model for estimating the daily upward longwave surface radiation flux from noaa-avhrr data," *International Journal of Remote Sensing*, vol. 14, no. 5, pp. 907–925, 1993.

[8] C. J. Neumann, "Global Overview - Chapter 1 Global Guide to Tropical Cyclone Forecasting," World Meteorological Organization, Tech. Rep., 1993.

[9] C. A. Senior and J. F. B. Mitchell, "Carbon dioxide and climate. the impact of cloud parameterization," *Journal of Climate*, vol. 6, no. 3, pp. 393–418, 1993.

[10] T. Suzuki, M. Tanaka, and T. Nakajima, "The microphysical feedback of cirrus cloud in climate change," *Journal of the Meteorological Society of Japan. Ser. II*, vol. 71, no. 6, pp. 701–714, 1993.

[11] J. J. Bates, X. Wu, and D. L. Jackson, "Interannual Variability of Upper-Troposphere Water Vapor Band Brightness Temperature," *Journal of Climate*, vol. 9, no. 2, pp. 427–438, 1996.

[12] B. Liebermann and C. A. Smith, "Description of a Complete (Interpolated) Outgoing Longwave Radiation Dataset," *Bulletin of the American Meteorological Society*, vol. 77, no. 6, pp. 1275–1277, Jun. 1996.

[13] W.-H. Lee, S. F. Iacobellis, and R. C. J. Somerville, "Cloud radiation forcings and feedbacks: General circulation model tests and observational validation," *Journal of Climate*, vol. 10, no. 10, pp. 2479–2496, 1997.

[14] J. C. L. Chan, J.-e. Shi, and C.-m. Lam, "Seasonal Forecasting of Tropical Cyclone Activity over the Western North Pacific and the South China Sea," *Weather and Forecasting*, vol. 13, no. 4, pp. 997–1004, 1998.

[15] K. E. Trenberth, A. Dai, R. M. Rasmussen, and D. B. Parsons, "The changing character of precipitation," *Bulletin of the American Meteorological Society*, vol. 84, no. 9, pp. 1205–1218, 2003.

[16] M. Chenoweth and C. Landsea, "The San Diego Hurricane of 2 October 1858," *Bulletin of the American Meteorological Society*, vol. 85, no. 11, pp. 1689–1698, 2004.

[17] K. B. Karnauskas, "The Africa Meridional OLR contrast as a diagnostic for Atlantic tropical cyclone activity and implication for predictability," *Geophysical Research Letters*, 2006.

[18] J. T. Fasullo and K. E. Trenberth, "The annual cycle of the energy budget. part i: Global mean and land–ocean exchanges," *Journal of Climate*, vol. 21, no. 10, pp. 2297–2312, 2008.

[19] J. W. Hanna, D. M. Schultz, and A. R. Irving, "Cloud-top temperatures for precipitating winter clouds," *Journal of Applied Meteorology and Climatology*, vol. 47, no. 1, pp. 351–359, 2008.

[20] H. Wang, J.-K. E. Schemm, A. Kumar, W. Wang, L. Long, M. Chelliah, G. D. Bell, and P. Peng, "A Statistical Forecast Model for Atlantic Seasonal Hurrican Activity Based on the NCEP Dynamical Seasonal Forecast," *Journal of Climate*, 2009.

[21] I. M. Held, M. Winton, K. Takahashi, T. Delworth, F. Zeng, and G. K. Vallis, "Probing the fast and slow components of global warming by returning abruptly to preindustrial forcing," *Journal of Climate*, vol. 23, no. 9, pp. 2418–2427, 2010.

[22] S. Kato, S. Sun-Mack, W. F. Miller, F. G. Rose, Y. Chen, P. Minnis, and B. A. Wielicki, "Relationships among cloud occurrence frequency, overlap, and effective thickness derived from calipso and cloudsat merged cloud vertical profiles," *Journal of Geophysical Research: Atmospheres*, vol. 115, no. D4, 2010.

[23] D. Lee and S. Choi, "Observation and numerical prediction of torrential rainfall over Korea caused by Typhoon Rusa (2002)," *Journal of Geophysical Research: Atmospheres (1984–2012)*, vol. 115, no. D12, Jun. 2010, ISSN: 2156-2202. DOI: 10.1029/2009JD012581.

[24] M. Winton, K. Takahashi, and I. M. Held, "Importance of ocean heat uptake efficacy to transient climate change," *Journal of Climate*, vol. 23, no. 9, pp. 2333–2344, 2010.

[25] E. S. Lim, C. J. Wong, K. Abdullah, and W. K. Poon, "Relationship between outgoing longwave radiation and rainfall in south east asia by using noaa and trmm satellite,"

in *2011 IEEE COLLOQUIUM ON HUMANITIES, SCIENCE AND ENGINEERING*, 2011, pp. 785–790.

[26] N.-Y. Kang and J. B. Elsner, "Consensus on Climate Trends in Western North Pacific Tropical Cyclones," *Journal of Climate*, vol. 25, no. 21, pp. 7564–7573, 2012.

[27] K. M. Cobb, N. Westphal, H. R. Sayani, J. T. Watson, E. Di Lorenzo, H. Cheng, R. L. Edwards, and C. D. Charles, "Highly Variable El Niño–Southern Oscillation Throughout the Holocene," *Science*, vol. 339, no. 6115, pp. 67–70, 2013.

[28] O. Geoffroy, D. Saint-Martin, G. Bellon, A. Voldoire, D. J. L. Olivié, and S. Tytéca, "Transient Climate Response in a Two-Layer Energy-Balance Model. Part II: Representation of the Efficacy of Deep-Ocean Heat Uptake and Validation for CMIP5 AOGCMs," *Journal of Climate*, vol. 26, no. 6, pp. 1859–1876, 2013.

[29] O. Geoffroy, D. Saint-Martin, D. J. L. Olivié, A. Voldoire, G. Bellon, and S. Tytéca, "Transient Climate Response in a Two-Layer Energy-Balance Model. Part I: Analytical Solution and Parameter Calibration Using CMIP5 AOGCM Experiments," *Journal of Climate*, vol. 26, no. 6, pp. 1841–1857, 2013.

[30] N. Oceanic and A. Administration. (2013). Seven Basins, [Online]. Available: `http://www.aoml.noaa.gov/phod/cyclone/data/seven.html`.

[31] J. B. Drake, *Climate Modeling for Scientists and Engineers*. SIAM, 2014.

[32] S. P. Sopko and R. J. Falvey, "Annual Tropical Cyclone Report," Joint Typhoon Warning Center, Tech. Rep., 2014.

[33] J. Wijnands, G. Qian, K. Shelton, R. Fawcett, J. Chan, and Y. Kuleshov, "Seasonal forecasting of tropical cyclone activity in the Australian and the South Pacific Ocean regions," *Mathematics of Climate and Weather Forecasting*, vol. 1, pp. 21–42, 2015.

[34] K. B. Karnauskas and L. Li, "Predicting Atlantic seasonal hurricane activity using outgoing longwave radiation over Africa," *Geophysical Research Letters*, 2016.

[35] K. Rays, M. Mohapatra, K. Chakravarthy, S. S. Ray, S. K. Singh, A. K. Das, B. A. M. Kannan, and B. K. Bandyopadhyay, "Hydro-meteorological aspects of tropical cyclone phailin in bay of bengal in 2013 and the assessment of rice inundation due to flooding," in *Tropical Cyclone Activity over the North Indian Ocean*, M. Mohapatra, B. Bandyopadhyay, and L. Rathore, Eds. Cham: Springer International Publishing, 2017, pp. 29–43.

[36] L. Zhang, T. Rechtman, K. B. Karnauskas, L. Li, J. P. Donnelly, and J. P. Kossin, "Longwave Emission Trends over Africa and Implications for Atlantic Hurricanes," *Geophysical Research Letters*, 2017.

[37] J. Hansen, M. Sato, R. Ruedy, L. Nazarenko, A. Lacis, G. A. Schmidt, G. Russell, I. Aleinov, M. Bauer, S. Bauer, N. Bell, B. Cairns, V. Canuto, M. Chandler, Y. Cheng, A. D. Genio, G. Faluvegi, E. Fleming, A. Friend, T. Hall, C. Jackman, M. Kelley, N. Kiang, D. Koch, J. Lean, J. Lerner, K. Lo, S. Menon, R. Miller, P. Minnis, T. Novakov, V. Oinas, J. Perlwitz, J. Perlwitz, D. Rind, A. Romanou, D. Shindell, P. Stone, S. Sun, N. Tausnev, D. Thresher, B. Wielicki, T. Wong, M. Yao, and S. Zhang, "Efficacy of climate forcings," *Journal of Geophysical Research: Atmospheres*, vol. 110, no. D18,

[38] R. N. B. Smith, "A scheme for predicting layer clouds and their water content in a general circulation model," *Quarterly Journal of the Royal Meteorological Society*, vol. 116, no. 492, pp. 435–460,

[39] Y. Sun, Z. Zhong, T. Li, L. Yi, S. J. Camargo, Y. Hu, K. Liu, H. Chen, Q. Liao, and J. Shi, "Impact of ocean warming on tropical cyclone track over the western north pacific: A numerical investigation based on two case studies," *Journal of Geophysical Research: Atmospheres*, vol. 122, no. 16, pp. 8617–8630,